Electronic Supplementary Material (ESI) for Catalysis Science & Technology.
This journal is © The Royal Society of Chemistry 2024

Supporting Information

Engineering selective CO_2 photoreduction by tailored interfacial design of P-modulated CuPc/B-C_3N_4 heterojunction for improved C_2H_4 selectivity

Imran Khan[a], Baoji Miao[a]*, Salman Khan[b], Amir Zada[c], Sharafat Ali[d], Muhammad Rizwan [e], Afsar Khan [f], Abdullah N. Alodhayb[g], Muhammad Ishaq Ali Shah[c],*

[a] Henan International Joint Laboratory of Nano-Photoelectric Magnetic Materials. School of Materials Science and Engineering, Henan University of Technology, Zhengzhou city, 450001, PR China.

[b] Key Laboratory of Functional Inorganic Materials Chemistry (Heilongjiang University), Ministry of Education, School of Chemistry and Materials Science, International Joint Research Center and Lab for Catalytic Technology, Harbin 150080, PR China.

[c] Department of Chemistry, Abdul Wali Khan University, Mardan, Khyber Pakhtunkhwa, 23200, Pakistan

[d] School of Physics, University of Electronic Science and Technology of China, Chengdu 610054, PR China.

[e] School of Energy Science and Engineering, Central South University, Changsha, 410083, PR China.

[f] School of Mineral Processing and Bioengineering, Central South University, 410083, Changsha, PR China

[g] Department of Physics and Astronomy, College of Science, King Saud University, Riyadh

Corresponding authors: Imran Khan (imrankhan@csu.edu.cn), and Baoji Miao (miaobaoji@foxmail.com)

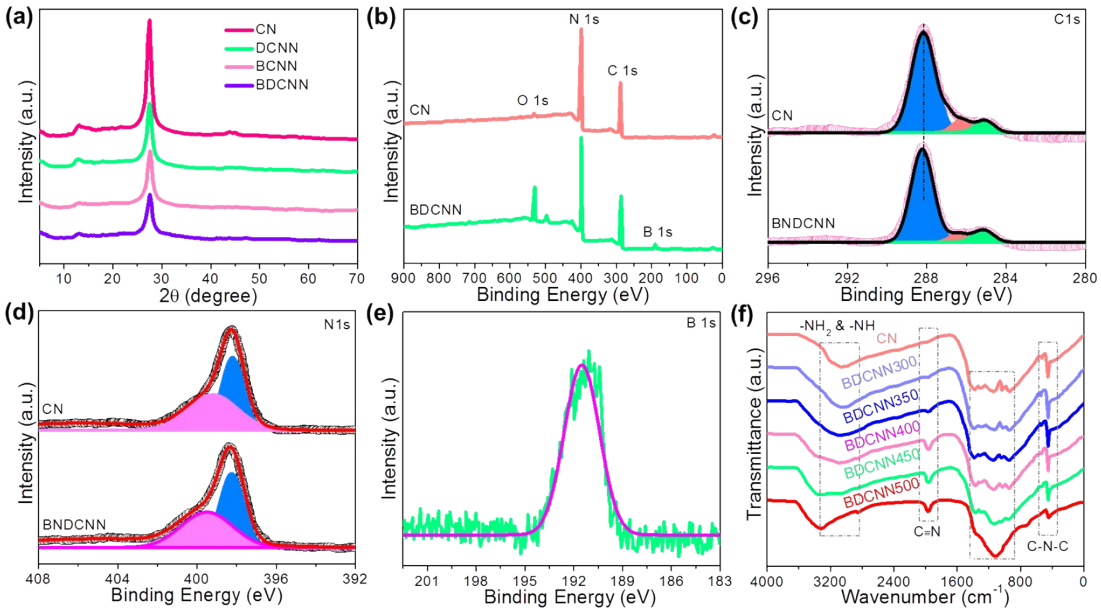

Figure 1. (a) XRD pattern spectra of prepared CN, DCNN, BCNN and BDCNN catalysts. (b) The survey XPS spectra of CN and BDCNNx, The corresponding high-resolution XPS spectra of (c) C 1s, (d) N 1s and (e) B 1s; (f) FTIR spectra of CN, and BDCNNx (x = 300, 350, 400, 450, 500).

The crystalline structures of the prepared materials were evaluated using XRD characterization. **Fig. S1a** illustrates that all the prepared catalysts exhibit two

characteristic diffraction peaks. The small peak at 13.9° corresponds to intralayer long-range atomic order (100), which is linked to the hydrogen bond in carbon nitride.[4] Additionally, the peak at 27.2° is attributed to interlayer periodic stacking (002) along the c-axis in carbon nitride.[5] The BDCNNx catalyst exhibits a decrease in the intensity of the (100) peak compared to the pristine CN catalyst, indicating partial disruption of hydrogen bonds in the framework. This weakened hydrogen bond effect leads to disordered periodic stacking of carbon nitride, resulting in a reduced (002) peak. An element analysis (EA) was conducted to investigate the elemental composition of BDCNNx. The results in Table S1 show that the catalyst contains 46.26% C, 47.25% N, and 1.851% H. Moreover, the molar ratio of C/N (0.98) is higher than the theoretical value of 0.75, implying the presence of surface N vacancies.

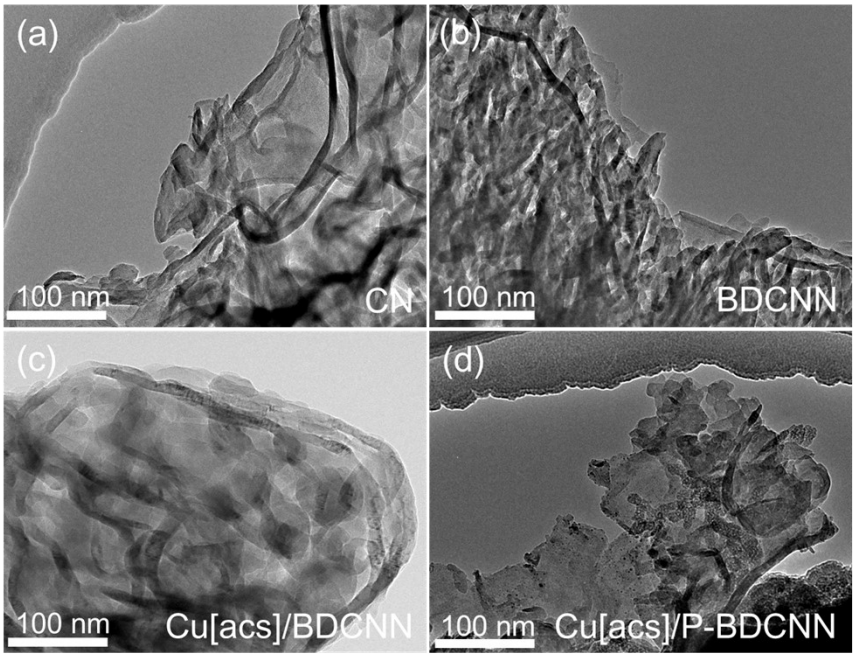

Figure S2. TEM images of (a) CN, (b) BDCNN, (c) Cu[acs]/BDCNN, (d) Cu[acs]/P-BDCNN.

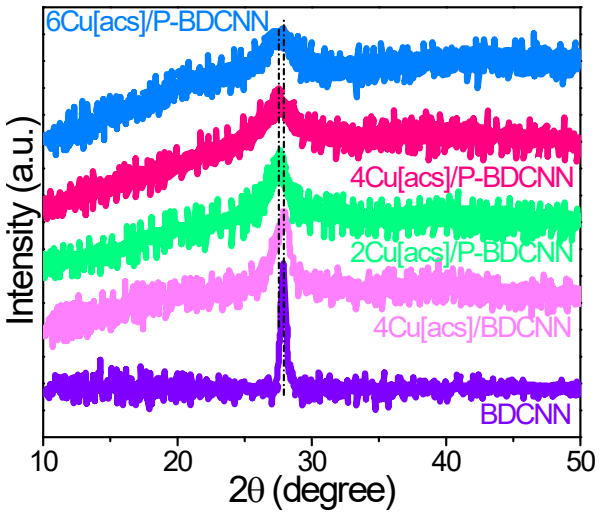

Figure S3. XRD patterns of BDCNN, 4Cu[acs]/BDCNN, 2Cu[acs]/P-BDCNN, 4Cu[acs]/P-BDCNN and 6Cu[acs]/P-BDCNN.

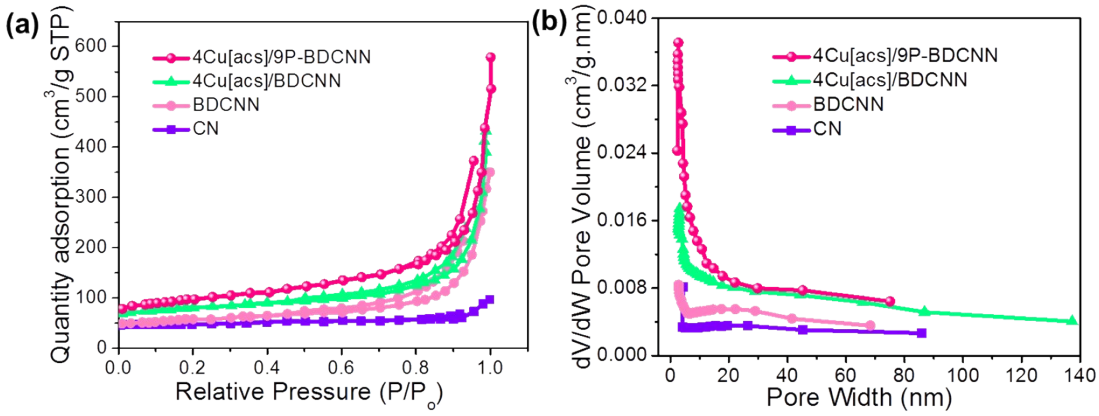

Figure S4. (a) N_2 adsorption-desorption isotherms and (b) pore size distribution for prepared CN, BDCNN, 4Cu[acs]/BDCNN and 4Cu[acs]/9P-BDCNN catalysts.

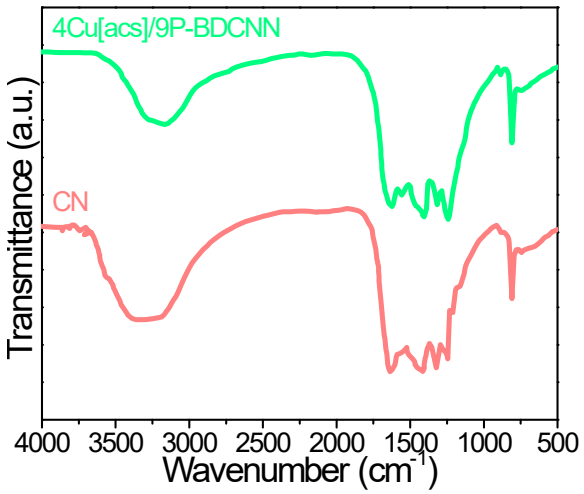

Figure S5. FTIR spectra of CN and 4Cu[acs]/9P-BDCNN.

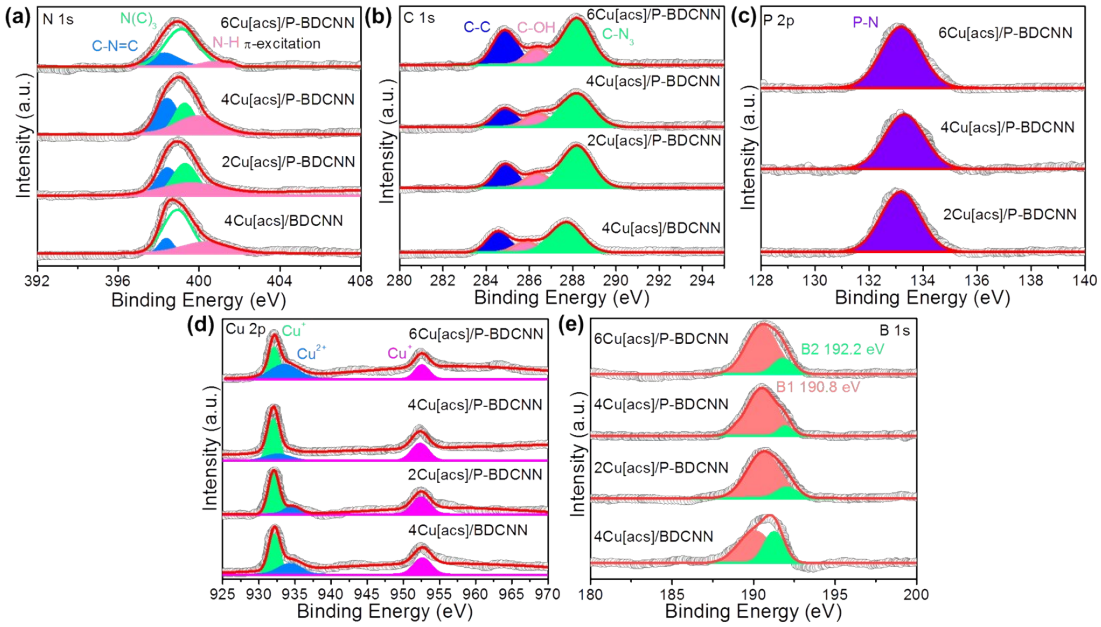

Figure S6. (a) The N 1s XPS spectra, (b) C 1s XPS spectra, (c) P 2p XPS spectra and (d) Cu 2p XPS spectra and (e) B 1s XPS spectra of the synthesized photocatalysts.

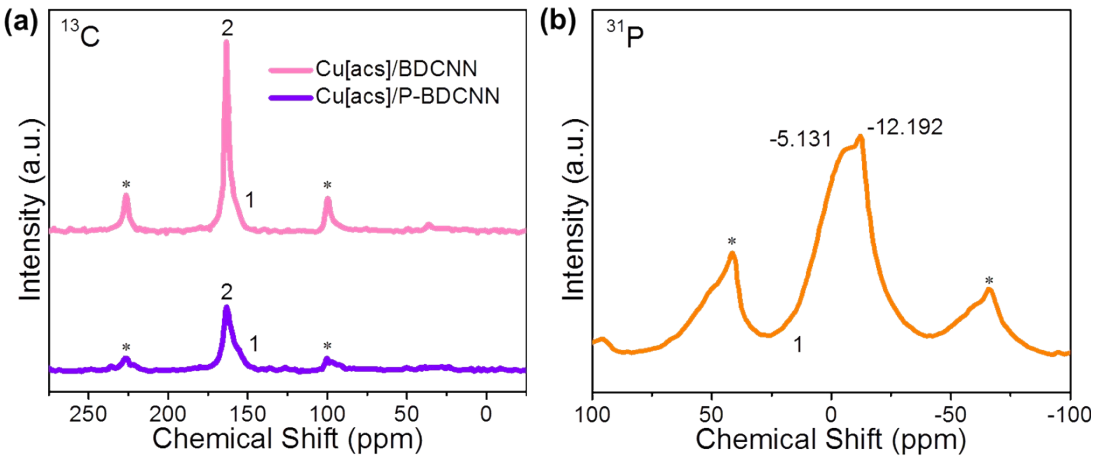

Figure S7. (a) Solid ^{13}C NMR spectra of Cu[acs]/BDCNN and Cu[acs]/P-BDCNN, (b) Solid ^{31}P NMR spectrum of Cu[acs]/P-BDCNN. Asterisk (□) indicates the spinning side bands.

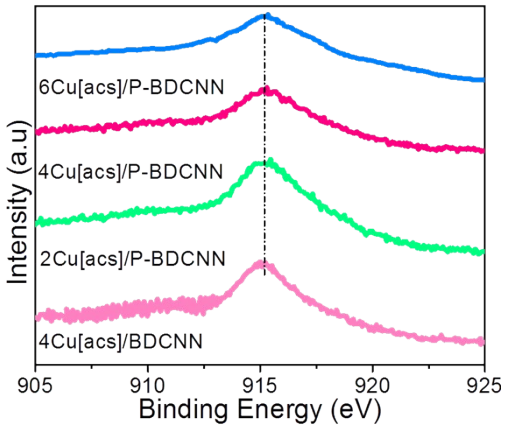

Figure S8. Cu LMM Auger spectra of 4[acs]/BDCNN, 2Cu[acs]/9P-BDCNN, 4Cu[acs]/9P-BDCNN, and 6Cu[acs]/9P-6BDCNN

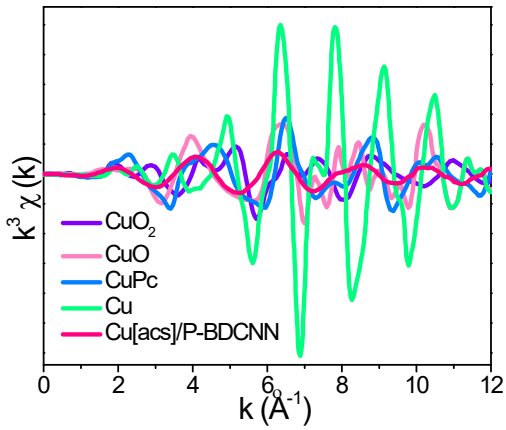

Figure S9. Extended X-ray absorption fine structure (EXAFS, k^3-weighted k-space) of 6Cu[acs]/9P-BDCNN

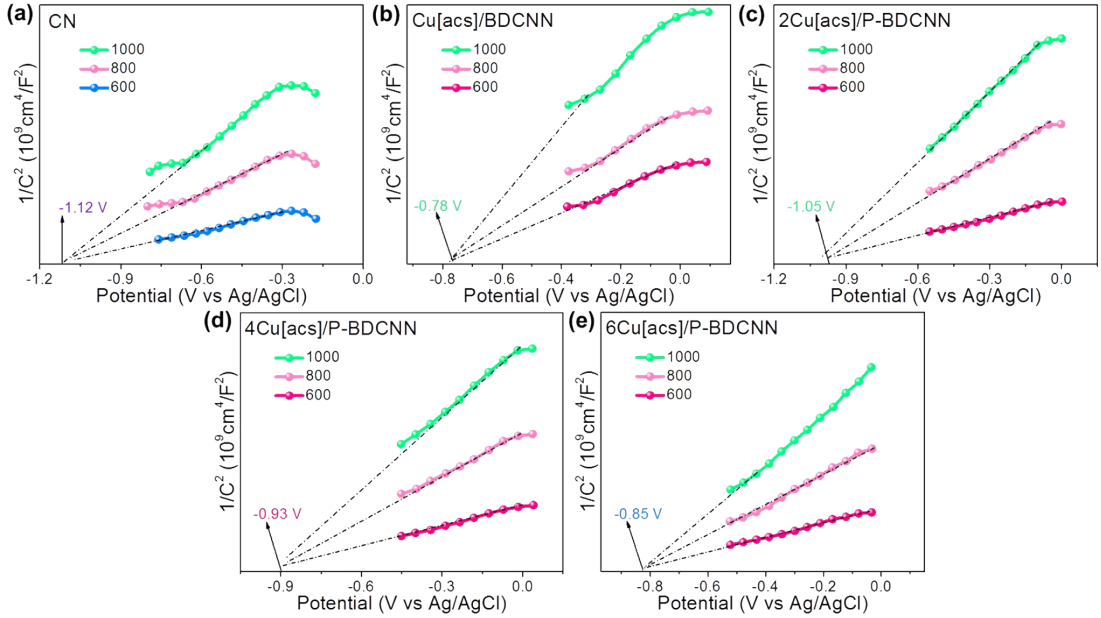

Figure S10. The Mott-Schottky plots of (a) CN, (b) Cu[acs]/BDCNN, (c) 2Cu[acs]/9P-BDCNN, (d) 4Cu[acs]/9P-BDCNN and (e) 6Cu[acs]/9P-BDCNN

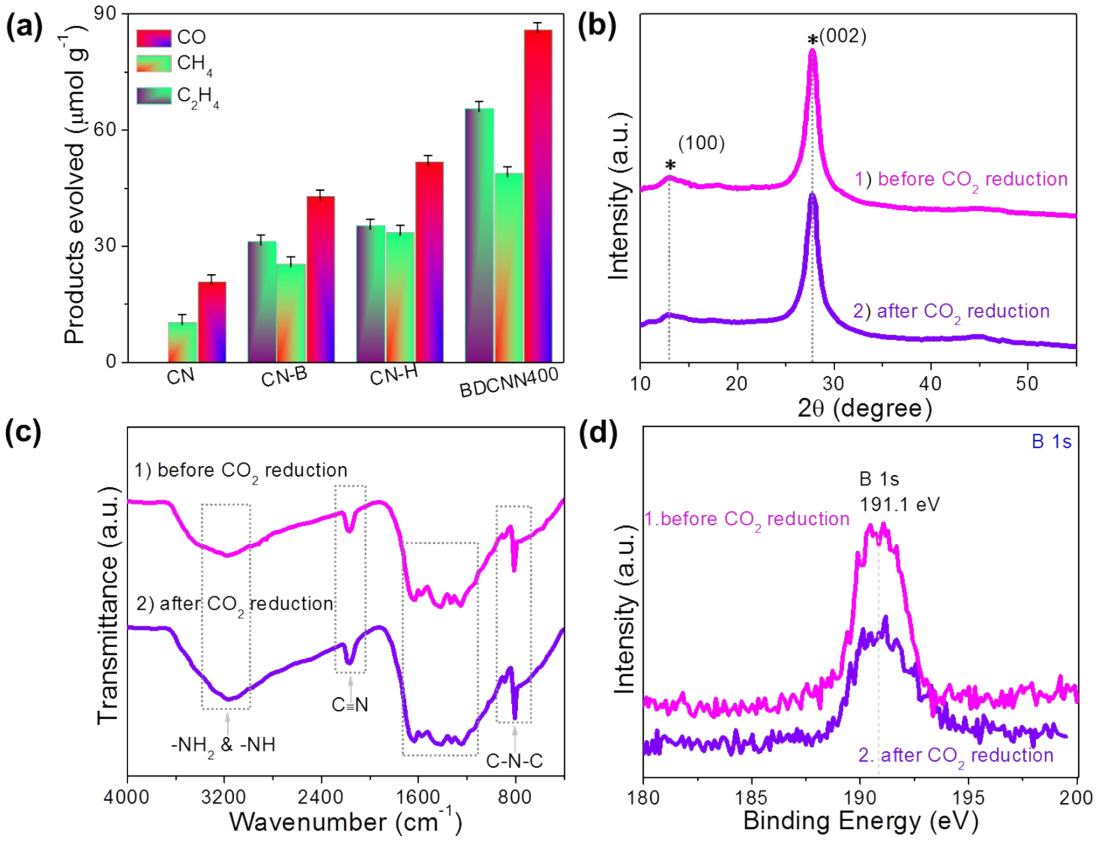

Figure S11. (a) Photocatalytic performance b) XRD diffractograms, c) FTIR spectra and d) high-resolution B1s XPS spectra of BDCNN400 1) before and 2) after the CO_2 reduction reaction.

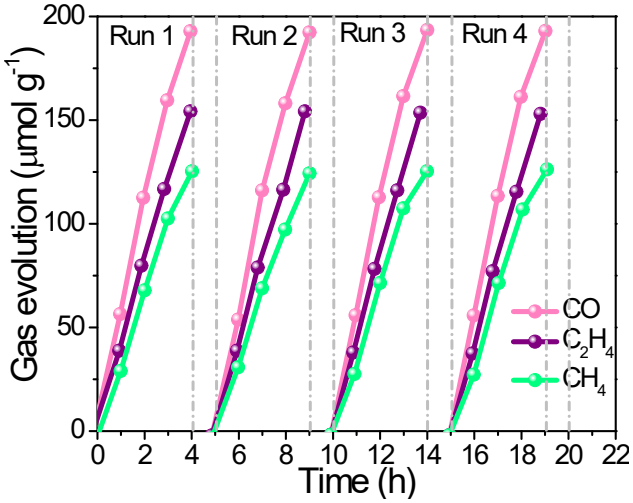

Figure S12. Reusability test of 4Cu[acs]/9P-BDCNN four consecutive runs of CO_2 reduction under visible-light irradiation

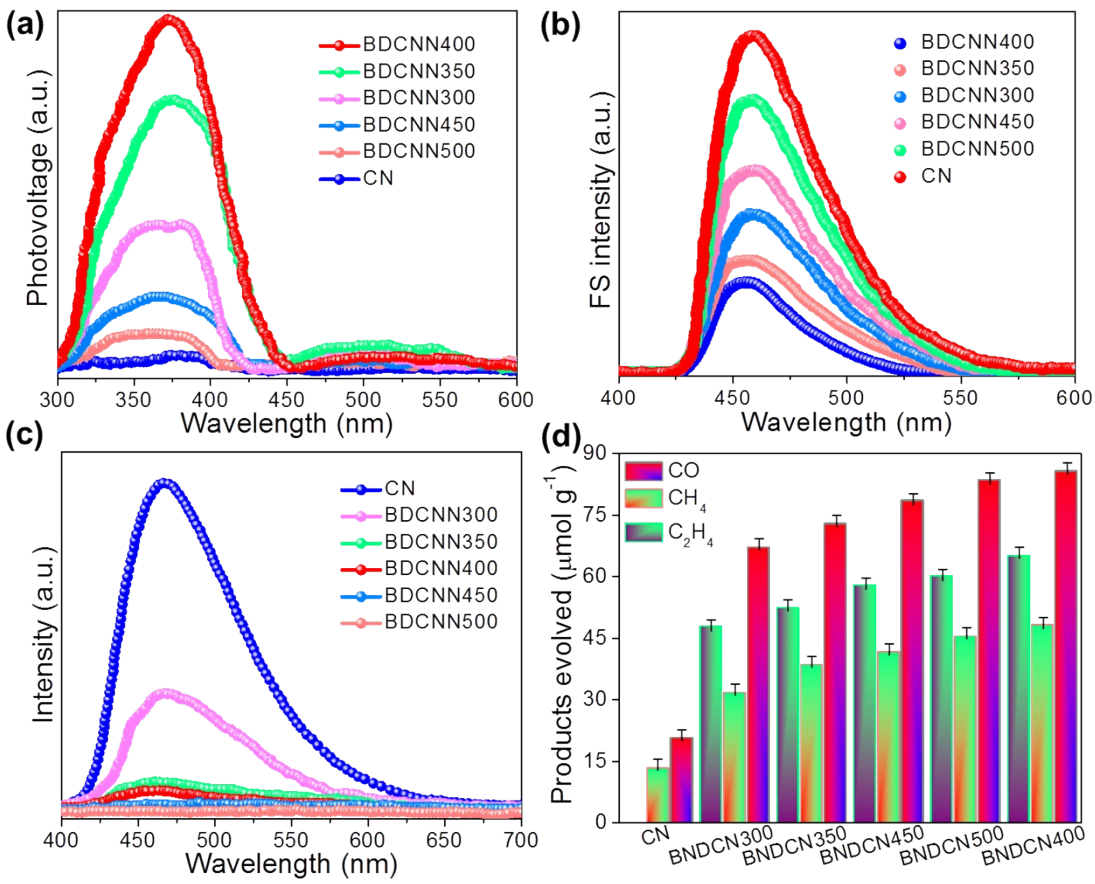

Figure S13. (a) SPS spectra, (b) fluorescence spectra related to the formed hydroxyl radicals under visible-light irradiation of BDCNN and XCoPc/BDCNN. (c) PL spectra and (d) Photocatalytic activities for CO_2 reduction reaction of CN and BDCNNx (x = 300, 350, 400, 450, 500) under visible-light irradiation.

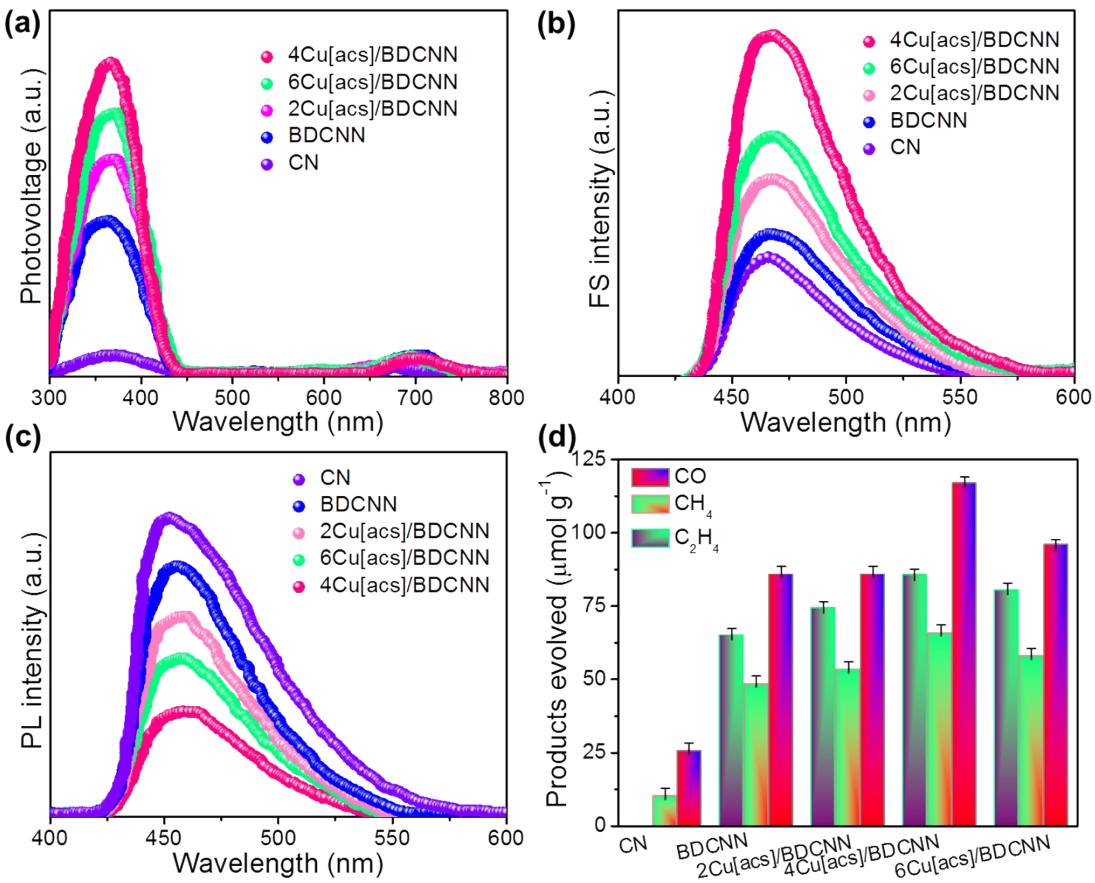

Figure S14. (a) SPS spectra (b) fluorescence spectra related to the formed hydroxyl radicals under visible-light irradiation (c) PL spectra and (d) Photocatalytic activities for CO_2 reduction reaction of CN, BDCNN and xCu[acs]/BDCNN (x = 2, 4, and 6) under visible-light irradiation.

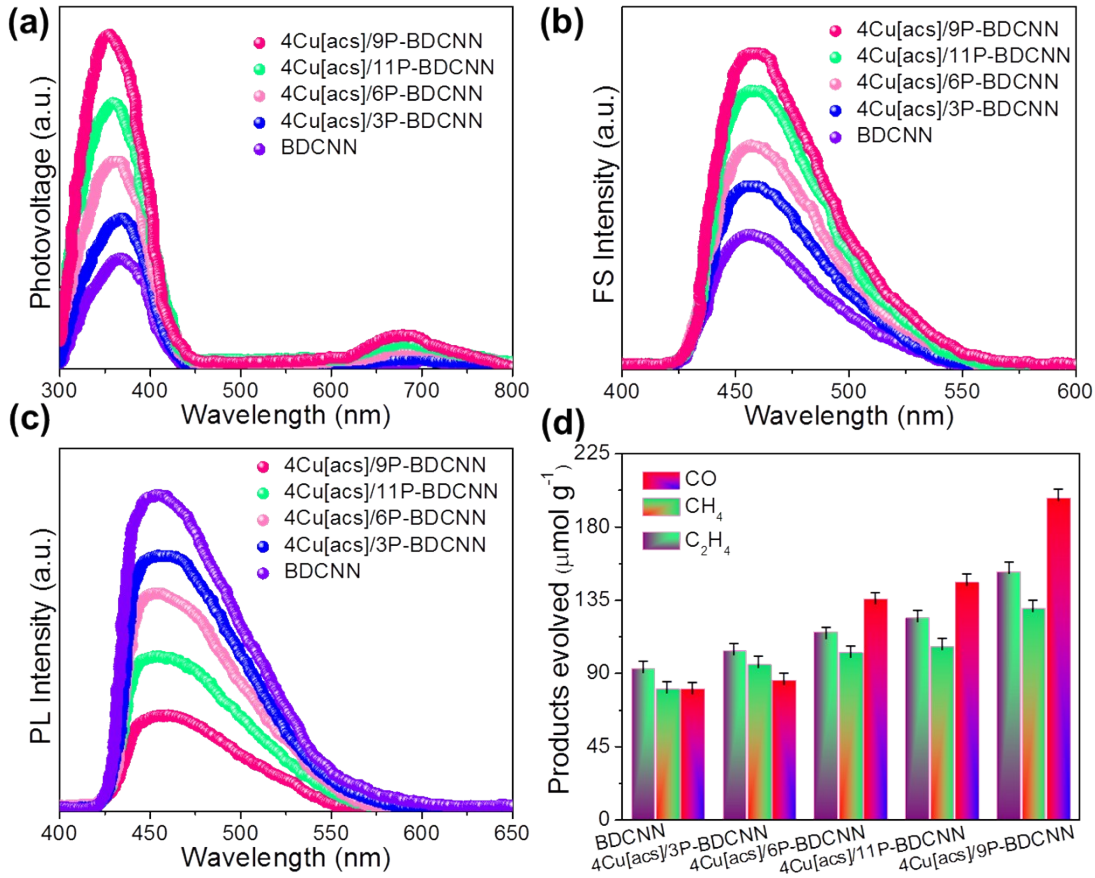

Figure S15. (a) SPS spectra (b) fluorescence spectra related to the formed hydroxyl radicals under visible-light irradiation (c) PL spectra and (d) Photocatalytic activities for CO_2 reduction reaction of CN, BDCNN and 4Cu[acs]/yP-BDCNN (y = 3, 6, 9 and 11) under visible-light irradiation.

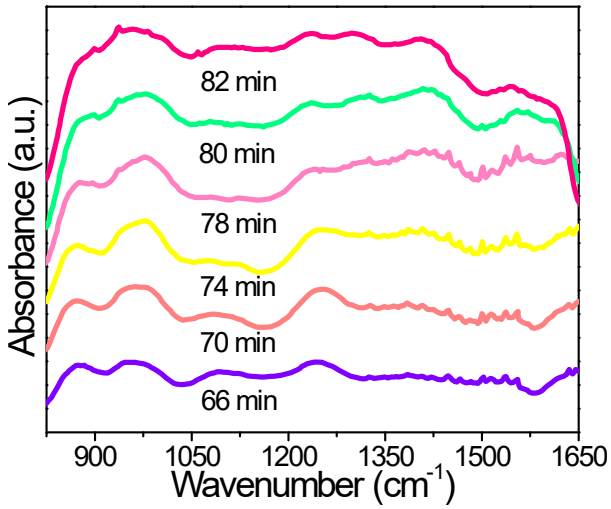

Figure S16. *In situ* DRIFTS spectra for detecting the reaction intermediates on 4Cu[acs]/9P-BDCNN in CO_2 photoreduction under 66~82 min simulated sunlight.

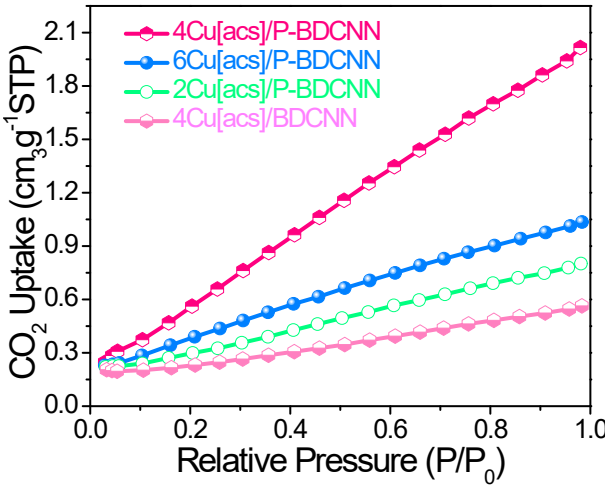

Figure S17. CO_2 adsorption isotherms for 4Cu[acs]/BDCNN, 2Cu[acs]/9P-BDCNN, 4Cu[acs]/9P-BDCNN and 4Cu[acs]/9P-BDCNN.

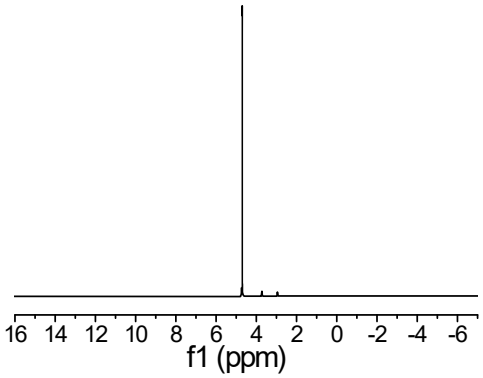

Figure S18. NMR spectrum of liquid products after 3 h CO_2 photoreduction over 4Cu[acs]/9P-BDCNN.

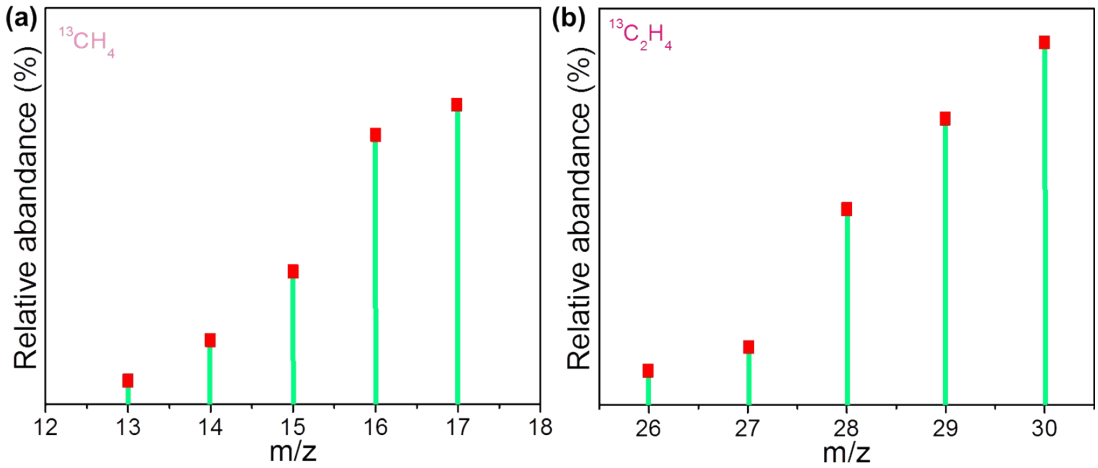

Figure S19. Mass spectra of $^{13}CH_4$ (a) and $^{13}C_2H_4$ (b) production over 4Cu[acs]/9P-BDCNN.

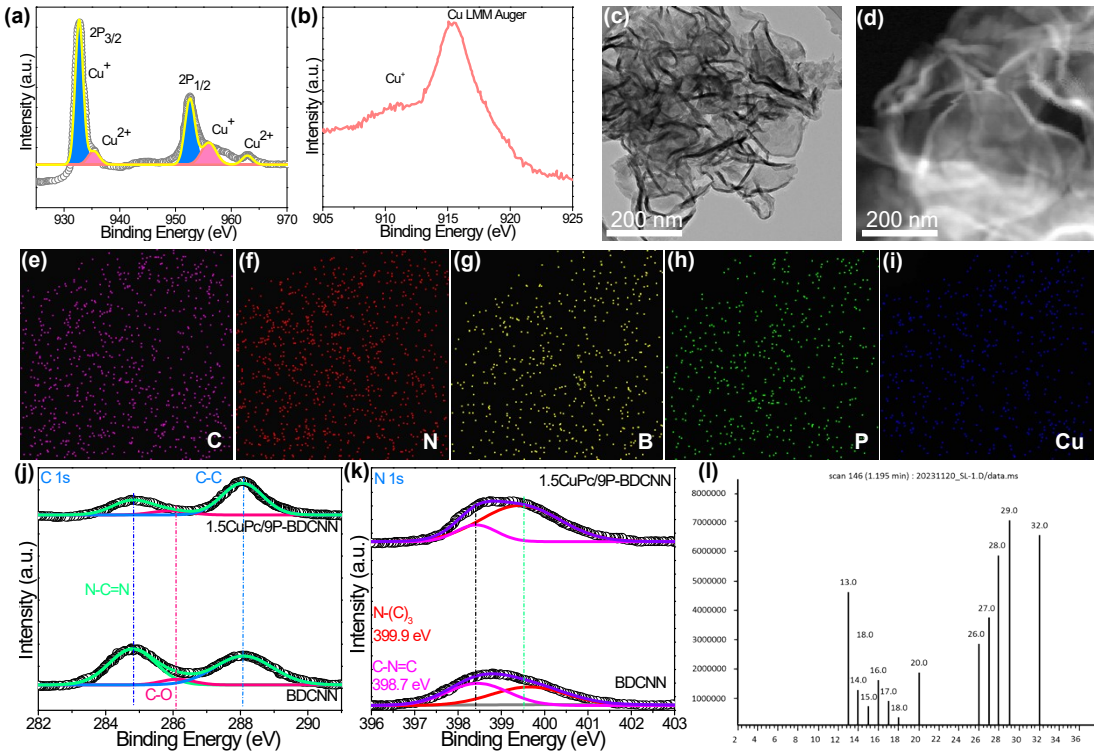

Figure S20. (a) Cu 2p XPS spectra, (b) Cu LMM Auger spectra, (c) TEM image and (d) HAADF-STEM image of 4Cu[acs]/9P-BDCNN and (e-i) EDS images of 4Cu[acs]/9P-BDCNN after four cycling tests.The corresponding high-resolution XPS spectra of (j) C 1s, (k) N 1s of BDCNN and 1.5CuPc/9P-BDCNN and (l) The online mass spectra of $^{13}CH_4$, $^{12}CH_4$, $^{13}C_2H_4$ and $^{13}C_2H_4$ of 1.5CuPc/9P-BDCNN.

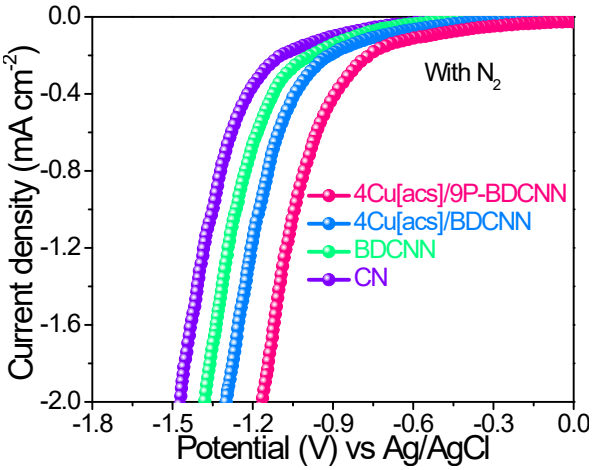

Figure. S21 Electrochemical reduction curves of CN, BDCNN, 4Cu[acs]/BDCNN. and 4Cu[acs]/9P-BDCNN, respectively, with CO_2 and N_2, bubbling system.

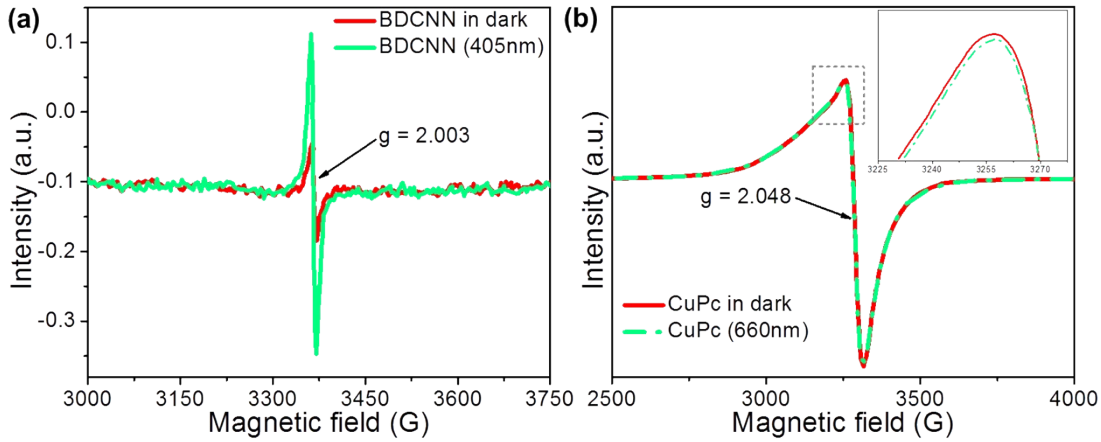

Figure. S22 EPR spectra of (a) BDCNN with 405 nm monochromatic light irradiation, (b) CuPc with 660 nm monochromatic light irradiation.

Table S1. C N, B, P and Cu contents (mol%) in g-C_3N_4, BNDCN and 1.5CuPc/9P-BDCNN according to elemental ICP analysis before and after CO_2 reduction reaction.

Samples	Before reduction reaction					After reduction reaction				
	N	C	B	Cu	P	N	C	B	Cu	P
g-C_3N_4	57.51	38.31	0	0	0	56.20	39.01	0	0	0
BDCNN300	54.78	38.01	00.03	0	0	53.62	37.21	0.015	0	0
BDCNN350	56.32	38.43	01.38	0	0	54.31	36.23	01.23	0	0
BDCNN400	52.65	36.06	03.90	0	0	49.13	35.12	03.72	0	0
BDCNN450	44.12	35.55	16.21	0	0	45.01	32.56	13.19	0	0
BDCNN500	38.75	31.76	10.16	0	0	35.62	31.03	10.61	0	0
4Cu[acs]/9P-BDCNN	43.16	37.02	03.79	0.18	0.03	44.01	36.03	03.45	0.17	0.014

Table S2. Binding energy of BDCNN, Cu[acs]/BDCNN and Cu[acs]/P-BDCNN with CH_2.

Material	BDCNN	Cu[acs]/BDCNN	Cu[acs]/P-BDCNN
E_b(eV)	-4.85	-5.24	-5.75

References

1. S. Grimme, *J Comput Chem*. 2006, 27, 1787-1799.
2. J. K. Norskov, J. Rossmeisl, A. Logadottir, L. Lindqvist, J. R. Kitchin, T. Bligaard, H. Jonsson, *J. Phys. Chem. B*. 2004, 108, 17886-17892.
3. J. P. Perdew, K. Burke, M. Ernzerhof, *Phys. Rev. Lett*. 1996, 77, 3865-3868.
4. C. Liang, H.P. Feng, H.Y. Niu, C.G. Niu, J.S. Li, D.W. Huang, L. Zhang, H. Guo, N. Tang, H.Y. Liu, 384 (2020) 123236.
5. C. Liang, C.G. Niu, H. Guo, D.W. Huang, X.J. Wen, S.F. Yang, G.M. Zeng, *Catal. Sci. Technol*. 8 (2018) 1161–1175